

Structure of Nanocrystalline Titania Ceramics Studied by X-ray Diffraction, Atomic Force Microscopy, and Thermal Phonon Kinetics

V. V. Ivanov*, S. N. Ivanov**, O. V. Karban***, A. V. Taranov**,
E. N. Khazanov**, and V. R. Khrustov*

* *Institute of Electrophysics, Ural Division, Russian Academy of Sciences,
Komsomol'skaya ul. 34, Yekaterinburg, 620049 Russia*

** *Institute of Radio Engineering and Electronics, Russian Academy of Sciences,
Mokhovaya ul. 11, Moscow, 125009 Russia*

*** *Physicotechnical Institute, Udmurt Scientific Center, Ural Division, Russian Academy of Sciences,
ul. Kirova 132, Izhevsk, 426000 Russia
e-mail: khazanov@nep.cplire.ru*

Received December 9, 2003; in final form, April 12, 2004

Abstract—The structure of TiO₂ nanocrystalline ceramics prepared from two types of nanopowders by shock compression followed by sintering in a conventional resistance furnace or via microwave heating is investigated by x-ray diffraction, x-ray photoelectron spectroscopy, atomic force microscopy, and thermal phonon kinetics. The results demonstrate that microwave sintering ensures a denser ceramic microstructure as compared to conventional sintering. Data are presented on the structure and thickness of intergranular films in the titania ceramics prepared by the two sintering processes.

INTRODUCTION

The ability to fabricate nanocrystalline titania ceramics with a grain size below 100 nm will markedly extend the application field of titania [1]. A viable approach to the fabrication of such ceramics is compaction of weakly agglomerated powders to a relatively high density (70–80% of theoretical density), followed by short-term sintering at reduced temperatures. The synthesis of nanocrystalline TiO₂ ceramics was reported by Bykov *et al.* [2]. Based on the phase composition and average grain sizes of anatase and rutile, they concluded that the preparation technique of the ceramic powder and the sintering procedure had a weak effect on the grain size of rutile and the density of the ceramics. At the same time, they found that the ceramics prepared by microwave sintering contained increased amounts of anatase and had greater microhardness in comparison with conventionally prepared ceramics.

In this paper, we report a comparative structural study of grains and grain boundaries in nanocrystalline TiO₂ ceramics prepared by conventional and microwave sintering. The characterization techniques included x-ray diffraction (XRD), x-ray photoelectron spectroscopy (XPS), atomic force microscopy (AFM), and thermal phonon kinetics.

EXPERIMENTAL, RESULTS, AND DISCUSSION

We studied high-density TiO₂ ceramics prepared from two types of nanopowders, one synthesized by chemical vapor deposition (NT-TiO₂, Nanophase Technologies Corp., USA) and the other by wire electroexplosion (P2-TiO₂, Institute of Electrophysics, Ural Division, Russian Academy of Sciences (RAS)). The powders were compacted to high density by magnetic shock compression. Owing to the high density of the green compacts, 3.1 to 3.3 g/cm³, these were sintered at reduced temperatures (≈850°C) for short periods of time (<15 min) either in a conventional resistance furnace (Institute of Electrophysics, Ural Division, RAS) or using microwave heating (Institute of Applied Physics, RAS).

The principal characteristics of the samples are listed in Table 1. The nature of the ceramic powder had an insignificant effect on the characteristics of the samples and will not be discussed here. The density and microhardness of the ceramics were determined by standard techniques.

Using XRD, we determined the percentages of rutile and anatase in the samples and the average crystallite sizes of these phases. Note that, with increasing density, the microhardness and grain size of the ceramics increase, while the anatase content decreases rapidly. The XRD patterns of the samples prepared by microwave sintering showed nonuniform broadening of dif-

Table 1. Characteristics of TiO₂ ceramics prepared by different sintering procedures

Sample no.	TiO ₂ powder	Sintering conditions	ρ_s , g/cm ³	Porosity, %	H_V , GPa	Percentages of rutile (R) and anatase (A)	Phase size, nm (XRD)	Crystallite size, nm (AFM)	State of grain boundaries (AFM)	D_{eff} , cm ² /s
1	P2-TiO ₂	850°C, 15 min*	3.86	11	–	–	–	50–100 (two distinct phases)	Incomplete formation of boundaries; rounded crystals, pores	–
2	P2-TiO ₂	850°C, 15 min	4.08	3.5	–	R, ≈100	125	300–500	Incomplete formation of boundaries	29
3	P2-TiO ₂	950°C, 0 min	4.14	2.2	12.5	R, 100	143	100–200	–	8.25
4	P2-TiO ₂	850°C, 15 min	4.20	0.8	11.9	R, 100	194	300–600 (one phase)	Sharp boundaries	27
5	NT-TiO ₂	30°C/min, 850°C, 13 min	4.18	1.3	13.4	R, 100	>300	300–500	Same as above	36–40
6	NT-TiO ₂	50°C/min, 850°C, 13 min	4.20	0.8	13.4	R, 100 A, traces	213	200–1000	Same as above	35
7	NT-TiO ₂	75°C/min, 850°C, 13 min	4.21	0.5	13.4	R, 100	>300	200–500	Same as above	40
8	NT-TiO ₂	50°C/min, 800°C, 5 min	4.19	0.95	13.7	R, 98 A, 2	162	100–250	Incomplete formation of boundaries	30
9	NT-TiO ₂	50°C/min, 600°C, 0 min	3.48	14.8	13.7	R, 19 A, 81	56 52	40–80 (two distinct phases, the dark phase prevails)	Rounded crystals, pores	–
10	NT-TiO ₂	50°C/min, 685°C, 1°C/min to 700°C, 0 min	4.01	4.7	12.7	R, 88 A, 12	103 66	100 (crystallite size of the dark phase; the light phase prevails)	–	20

Note: Samples 1–4 were prepared by conventional sintering, and samples 5–10 were prepared using microwave heating.

* Holding time at the specified temperature.

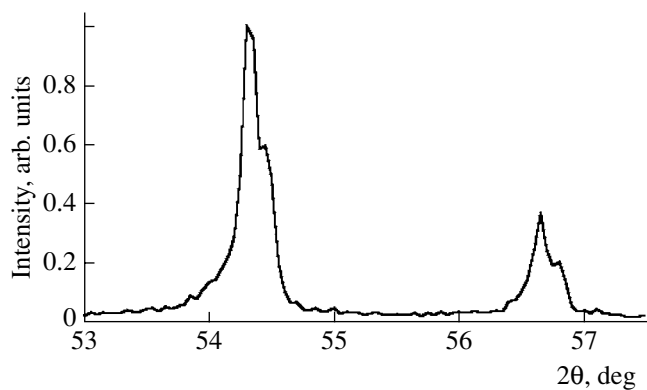


Fig. 1. Portion of the XRD pattern from sample 7 (micro-wave sintering).

fraction peaks, with small-angle tails (Fig. 1). One possible explanation for this finding is that the density of oxygen-related defects depends on the crystallite size. Fitting with Pearson-7 functions showed that each diffraction peak consisted of two components differing in width and angular position. Therefore, it seems likely that the samples contained two forms of rutile, differing in crystallite size and lattice parameters. For the rutile with a crystallite size of 150 nm, the lattice parameters were determined to be $a = 4.592 \text{ \AA}$ and $c = 2.959 \text{ \AA}$ ($a = 4.5933 \text{ \AA}$ and $c = 2.9592 \text{ \AA}$ according to JCPDS PDF data). The lattice parameters of the finer particle rutile (26 nm) are $a = 4.606 \text{ \AA}$ and $c = 2.964 \text{ \AA}$. It seems likely that the finer crystallites reside at the boundaries between the coarser crystallites.

AFM measurements were carried out on freshly fractured surfaces (all of the samples showed intercrystalline fracture) in a semicontact mode, using a P47-

MDT scanning probe microscope (NT-MDT, Zelenograd). The spatial resolution was several nanometers, which allowed us to obtain reliable structural data.

Topographic AFM studies were supplemented with phase contrast imaging. Phase contrast images are generated owing to changes in the phase of cantilever vibrations during scanning. Since the phase shift is very sensitive to the mechanical tip-sample interaction, phase contrast images provide information about the elastic properties of the sample surface and allow one to assess the structural homogeneity of the material [3, 4]. In this work, phase contrast imaging was used to reveal crystallite boundaries and the spatial distribution and morphology of anatase and rutile.

The grain size of the samples prepared by conventional sintering was found to increase with sintering temperature and time (Table 1). The samples contained agglomerates of grains up to 1.5 μm in size. The topographic image of a fracture surface of sample 1 in Fig. 2a shows two groups of crystallites: less than 50 nm and more than 100 nm in size. Phase contrast AFM imaging reveals two phases on the fracture surface, which appear as dark and light areas (Fig. 2b). Taking into account XRD results, we believe that these phases are anatase and rutile. The TiO_2 polymorphs were identified using quantitative x-ray phase analysis data. We also took into account the fact that metastable phases typically have a smaller crystallite size [5]. Under ordinary conditions, the critical crystallite size for the anatase-rutile phase transition is on the order of 50 nm: anatase is stable at smaller crystallite sizes and rutile is stable above this level. This allows us to identify the dark grains as anatase and the light grains as rutile. Note that, in all of the samples prepared by conventional sintering, especially in those containing ana-

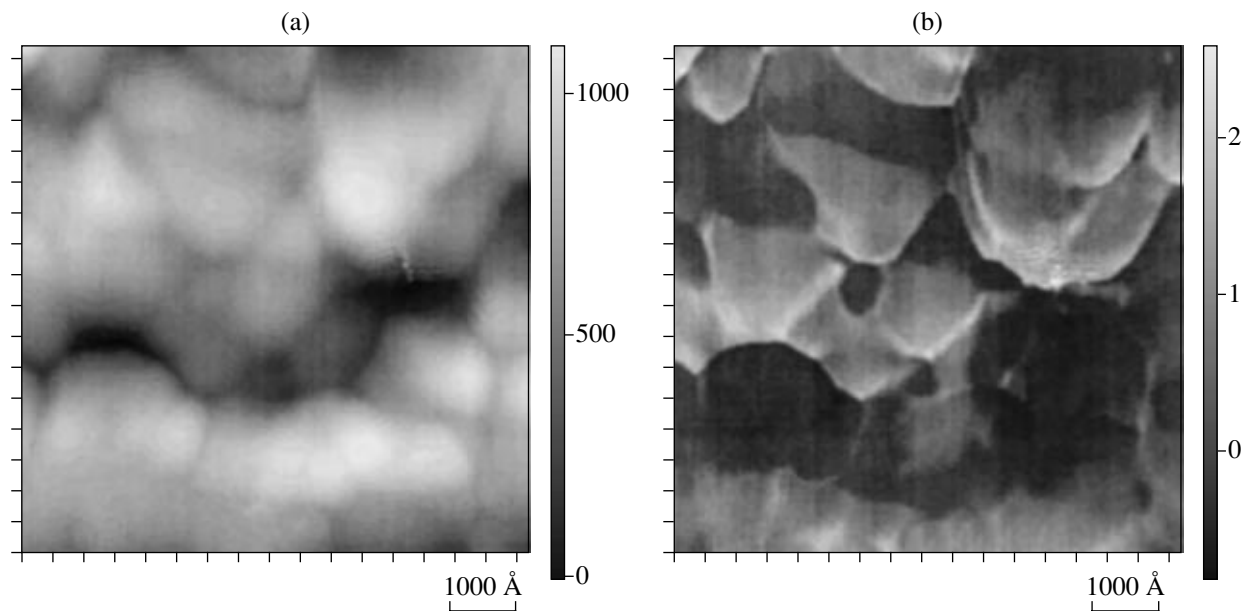


Fig. 2. (a) Topographic and (b) phase contrast AFM images of a fracture surface of sample 1 (conventional sintering).

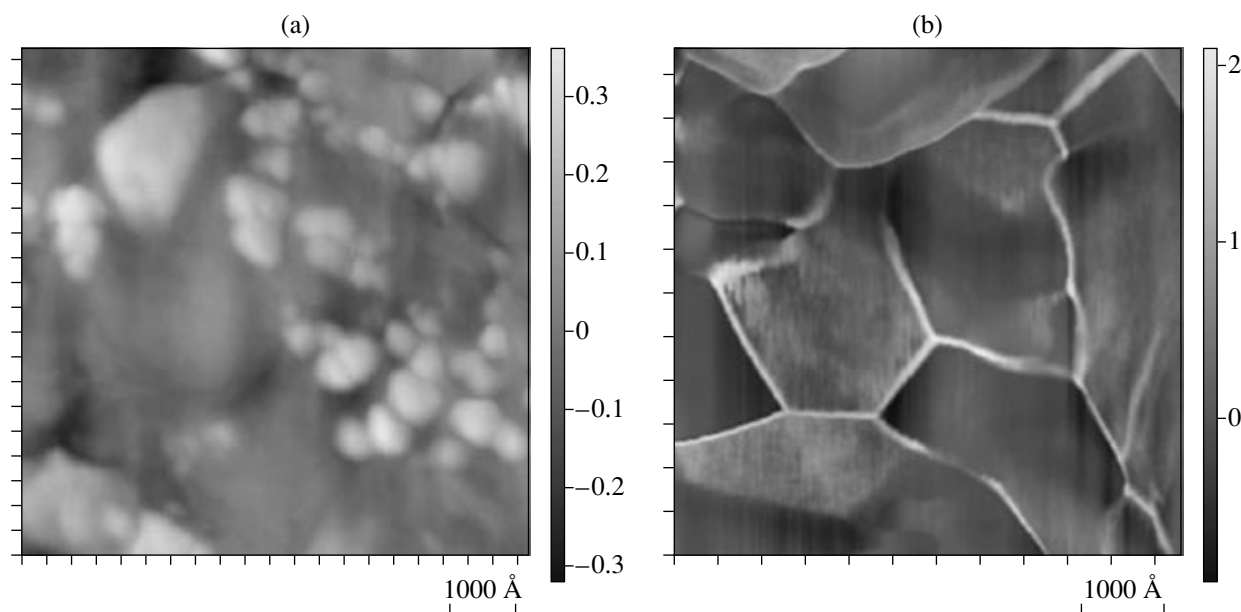


Fig. 3. Phase contrast images of fracture surfaces of samples (a) 9 and (b) 7 (microwave sintering).

tase, the formation of grain boundaries did not reach completion: the grains had a rounded shape, and we observed nanopores in three-grain junctions.

The samples prepared by microwave sintering had more perfect grain boundaries. At sintering temperatures below 800°C (samples 9, 10), we also observed two phases on fracture surfaces (the percentages of anatase and rutile correlated with XRD data). The two-phase samples had loose grain boundaries (Fig. 3a). Increasing the temperature (microwave power) to 850°C (samples 6, 7) led to grain growth and stabilization of grain boundaries via the formation of intergranular films (Fig. 3b) differing in elastic properties from the grain bulk. The observed contrast suggests that these films have increased rigidity [3].

Surface analysis by XPS was carried out on an ES-2401 spectrometer. It was found that the intergranular phases contained, in addition to titanium and oxygen, significant levels of carbon. High-temperature sintering leads to the formation of TiO, Ti₂O₃, and graphitic carbon in the surface region of the grains (Table 2, samples 1, 4). In the samples prepared by microwave sintering, a carbide-like phase is formed, and the Ti₂O₃ con-

tent of the surface layer decreases owing to the reaction Ti₂O₃ → TiO (samples 5, 9). In conjunction with the presence of carbides, this may stabilize the intergranular film and increase its rigidity.

It follows from the XPS data that, in the ceramics prepared by the two sintering processes, the intergranular film is no less than 8 nm in thickness.

Consider now the thermal phonon kinetics results obtained at liquid-helium temperatures. The principle of the “heat-pulse” method is as follows: A gold film evaporated onto one side of a platelike sample is heated by a short ($\approx 10^{-7}$ s) current pulse and serves as an injector of nonequilibrium phonons into the sample. To the other side of the plate is applied an Sn bolometer in the form of a meander 0.3×0.25 mm² in area. The working point of the bolometer is shifted by a magnetic field (≈ 16 kA/m), which makes it possible to examine the scattering of nonequilibrium phonons in the sample in the range 1.7–3.8 K. The heater power must be low enough that the thermostat (bath) temperature, with a nearly Planckian frequency distribution, can be ascribed to the injected phonons.

When the heat-pulse method is applied to ceramic materials [6], it is assumed that the mean free path of thermal phonons is much greater than the grain size of the ceramic, $l \gg R$, which is the case at low measurement temperatures if the material has a sufficiently perfect structure (Figs. 2, 3). In this situation, the scattering of nonequilibrium phonons is governed by the properties of grain boundaries and, at a large sample thickness, $L \gg R$, in the diffusive phonon transport regime, the peak-signal time is given by

$$t_{\max} \cong L^2/D_{\text{eff}}, \quad D_{\text{eff}} = v_s R f_{\omega} \frac{\Sigma}{S}, \quad (1)$$

Table 2. Surface composition of TiO₂ grains (XPS data)

Sample no.	Molar percent				
	TiO ₂	TiO	Ti ₂ O ₃	graphite	carbide
1	12.7	4.5	2.3	80.5	–
4	30.0	3.0	12.0	54.8	–
9	23.7	4.7	3.0	52.6	15.9
5	34.2	5.8	5.3	46.8	7.9

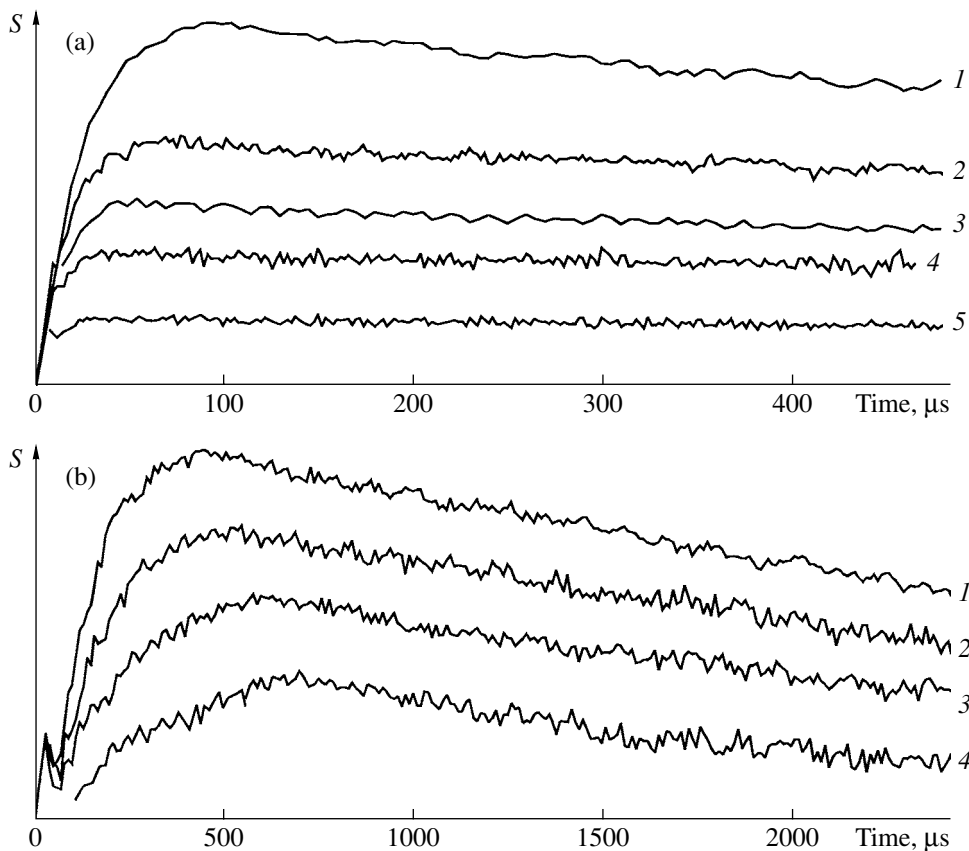


Fig. 4. Time dependences of the nonequilibrium phonon signal for TiO_2 ceramics: (a) sample 5 ($L = 0.06$ cm), $T = (1)$ 3.83, (2) 3.65, (3) 3.44, (4) 3.11, (5) 2.81 K; (b) sample 3 ($L = 0.061$ cm), $T = (1)$ 3.83, (2) 3.65, (3) 3.46, (4) 3.05 K.

where v_s is the sound velocity in the grains of the ceramic, S is surface area of the sample, Σ is the total contact area per grain, and f_ω is the probability that a phonon of frequency ω will pass through the contact. The Σ/S ratio represents the influence of grain-boundary porosity on phonon diffusion. For the ceramic samples used in our experiments (Table 1), it is reasonable to take $\Sigma/S \approx 1$. The estimated sound velocity is $v_s \approx 6 \times 10^5$ cm/s [7]. Thus, the way in which the effective phonon diffusivity D_{eff} varies with temperature, grain size, and the properties and area of grain boundaries provides detailed information about the ceramic material.

Figure 4 shows the heat-pulse curves for samples 3 (conventional sintering) and 5 (microwave sintering) at different temperatures. For both samples, the curves are bell-shaped, with a well-observed maximum, characteristic of the diffusive transport of injected phonons. Note that, in the case of the ceramics prepared by microwave sintering, the peak-signal time τ_{max} increases with temperature, $\tau_{\text{max}} \sim T^5$, in contrast to that in the samples prepared by conventional sintering: $\tau_{\text{max}} \sim T^{-2}$.

Earlier, Barabanenkov *et al.* [8] examined the dependence of $D_{\text{eff}} \approx L^2/\tau_{\text{max}}$ on the grain size of Al_2O_3 ,

ZrO_2 , and $\text{ZrO}_2\text{-Al}_2\text{O}_3$ ceramics (Fig. 5). According to their results, $D_{\text{eff}} \sim R$ for R varying over two orders of magnitude, in full accord with Eq. (1). Estimates from their data yield $\Sigma/S \approx 1$ and $f_\omega \approx 0.8\text{--}0.9$. We believe that, in the case of high-quality ceramics from other materials, deviations from those data (Fig. 5) are due to differences in the mean phonon velocity and the perfection of grain boundaries, that is, in the values of Σ/S and f_ω , appearing in Eq. (1).

The 3.8-K phonon diffusivities in the nanocrystalline TiO_2 ceramics prepared by the two sintering procedures fall close to curve 1 (Fig. 5). With allowance made for the reduction in mean phonon velocity by about a factor of 1.25, the differences in the characteristics of grain boundaries are insignificant. Thus, phonon diffusion in the samples studied here is governed by the properties of grain boundaries rather than by the bulk properties, since $D \sim R$. Consider now the temperature dependence of phonon diffusivity. For the TiO_2 ceramics prepared by microwave sintering, we find $\tau_{\text{max}} \sim T^5$. This temperature variation of D_{eff} is characteristic of phonon scattering by an amorphous intergranular film containing two-level systems, which offer a channel for strong anharmonic phonon scattering [9]. The density of localized soft vibrational states in such

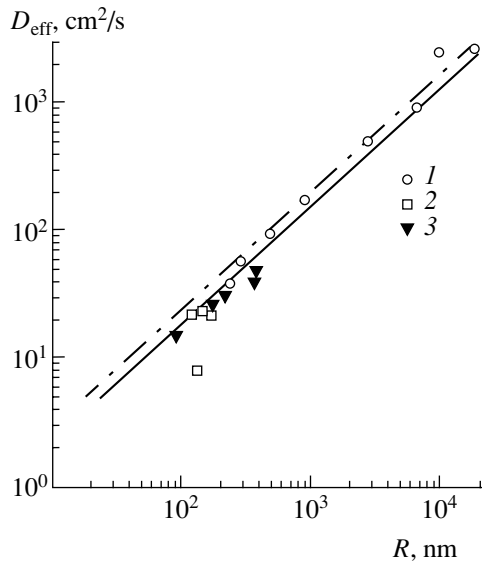


Fig. 5. Effective phonon diffusivity as a function of average grain size for ceramic samples at 3.81 K: (1) Al_2O_3 , ZrO_2 , and related composites [8]; (2, 3) TiO_2 ceramics prepared by conventional and microwave sintering, respectively. Deviations from curve 1 are associated with a lower mean phonon velocity.

layers may be very high [10, 11]. This makes it possible to achieve qualitative agreement between the model and experimental data on the phonon transport at ~ 10 K in thin glassy layers in which the phonon mean free path is a strong function of frequency (temperature) [12], which leads to a strong temperature variation of D_{eff} . It seems likely that the effective phonon scattering in the TiO_2 ceramics prepared by microwave sintering is due to the formation of glassy carbides and the associated two-level systems in the intergranular layer (Table 2). The thickness of the intergranular layer is difficult to estimate from the above data for lack of any tractable model. In view of this, we restrict the discussion to XPS data.

In the samples prepared by conventional sintering, $D_{\text{eff}} \sim T^{-2}$, which is consistent with the presence of an intergranular layer in which phonon transport is governed by acoustic matching [8]. In such a system, the T^{-2} behavior of D_{eff} is possible at $ql_{\text{gb}} \approx 1.5\text{--}2.0$, where q is the magnitude of the wavevector of the acoustic phonon and l_{gb} is the thickness of the intergranular layer. Taking $q \approx 2 \times 10^6 \text{ cm}^{-1}$, we obtain $l_{\text{gb}} \approx 7\text{--}10 \text{ nm}$. This value of l_{gb} correlates with the above XPS results for our ceramic samples.

The AFM and XPS data for the samples prepared by microwave sintering attest to more rigid, multiphase intergranular layers, which is also clearly evidenced by phonon kinetics experiments. Note also that the H_V of these samples slightly exceeds that of the ceramics prepared by conventional sintering, which correlates well with our findings on the structure of grain boundaries.

CONCLUSIONS

Studies of nonequilibrium phonon transport in TiO_2 ceramics, in combination with AFM, XPS, and XRD, provide detailed information about the structure and thickness of intergranular films in ceramics prepared by different sintering processes.

ACKNOWLEDGMENTS

We are grateful to O.M. Kanunnikova for measuring the x-ray photoelectron spectra and helpful discussions.

This work was supported by the Russian Foundation for Basic Research, grant no. 03-02-16233.

REFERENCES

1. Averbach, R.S., Hoefler, H.J., Hahn, H., and Logas, J.C., Sintering and Grain Growth in Nanocrystalline Ceramics, *Nanostruct. Mater.*, 1992, vol. 1, pp. 173–178.
2. Bykov, Yu., Eremeev, A., Egorov, S., *et al.*, Sintering of Nanostructural Titanium Oxide Using Millimeter-Wave Radiation, *Nanostruct. Mater.*, 1999, vol. 8, pp. 115–118.
3. Ahn, H.-S., Chizik, S.A., Dubravin, A.M., *et al.*, Application of Phase Contrast Imaging Atomic Force Microscopy to Tribofilms on DLC Coatings, *Wear*, 2001, vol. 249, pp. 617–625.
4. Karban, O.V. and Khasanov, O.L., Investigation of Zirconia Nanoceramics Microstructure, *Phys. Low-Dimens. Struct.*, 2003, vol. 2/3, pp. 297–308.
5. Groza, J.R., Sintering of Nanocrystalline Powders, *Int. J. Powder Metall.*, 1999, vol. 35, no. 7, pp. 59–66.
6. Ivanov, S.N., Kozorezov, A.G., Taranov, A.V., and Khazanov, E.N., Nonequilibrium Phonon Transport in Ceramic Materials, *Zh. Eksp. Teor. Fiz.*, 1992, vol. 102, no. 2 (8), pp. 600–617.
7. *Akusticheskie kristally* (Acoustic Crystals), Shaskol'skaya, M.P., Ed., Moscow: Nauka, 1982, pp. 231–242.
8. Barabanenkov, Yu.N., Ivanov, V.V., Ivanov, S.N., *et al.*, Heat Pulse Study of Alumina- and Zirconia-Based Ceramics, *Zh. Eksp. Teor. Fiz.*, 2001, vol. 119, no. 3, pp. 546–555.
9. Levinson, I.B., Temperatures below 1 K in Dielectric Glasses, *Pis'ma Zh. Eksp. Teor. Fiz.*, 1983, vol. 37, no. 3, pp. 157–159.
10. Kozub, V.I., Rudin, A.M., and Schober, H., Nonequilibrium Phonon Transport in Amorphous Layers, *Phys. Rev.*, 1994, vol. 50, no. 9, pp. 6032–6046.
11. Kozub, V.I. and Rudin, A.M., Nonequilibrium Phonon Transport in Unstable Systems, *Fiz. Tverd. Tela* (S.-Peterburg), 1996, vol. 38, no. 2, pp. 3337–3378.
12. Scherg, G.P., Gartner, R., Berberich, P., and Kinder, H., Dispersion and Scattering of Monochromatic Phonons in Thin Amorphous PMMA-Films, *Phonon Scattering Condens. Matter*, 1992, vol. 7, pp. 266–268.